International Journal of Pharmaceutics 624 (2022) 122003

Contents lists available at ScienceDirect

International Journal of Pharmaceutics

journal homepage: www.elsevier.com/locate/ijpharm

Pharmacokinetic control on the release of antimicrobial drugs from pH-responsive electrospun wound dressings

Laura Miranda-Calderon [a,b], Cristina Yus [a,b], Guillermo Landa [a,b], Gracia Mendoza [c,d], Manuel Arruebo [a,b,c,*], Silvia Irusta [a,b,c,*]

[a] Instituto de Nanociencia y Materiales de Aragón (INMA), CSIC-Universidad de Zaragoza, Zaragoza 50009, Spain
[b] Department of Chemical Engineering, University of Zaragoza, Campus Río Ebro-Edificio I+D, C/ Poeta Mariano Esquillor S/N, 50018 Zaragoza, Spain
[c] Networking Research Center on Bioengineering, Biomaterials and Nanomedicine, CIBER-BBN, 28029-Madrid, Spain
[d] Aragon Health Research Institute (IIS Aragon), 50009 Zaragoza, Spain

ARTICLE INFO

Keywords:
Electrospinning
Eudragit®
pH-responsive
Drug delivery
Wound dressing

ABSTRACT

The acidic pH of healthy skin changes during wound healing due to the exposure of the inner dermal and subcutaneous tissue and due to the potential colonization of pathogenic bacteria. In chronic non-healing wounds, the pH values vary in a wide pH range but the appearance of an alkaline shift is common. After a wound is incurred, neutral pH in the wound bed is characteristic of the activation of the cascade of regenerative and remodeling processes. In order to adjust drug release to the specific pH of the wound, herein, drug-loaded wound dressings having pH-responsiveness containing antiseptics and antibiotics and exerting different release kinetics in order to have a perfect match between the drug release kinetics, and the pH conditions of each wound type, were developed. We have fabricated drug-loaded electrospun nanofibers loaded with the antiseptic chlorhexidine, with the broad-spectrum antibiotic rifampicin, and with the antimicrobial of natural origin thymol, using the pH-dependent methacrylic acid copolymer Eudragit® L100-55, which dissolves at pH > 5.5; those drugs were loaded within Eudragit® S100, which dissolves at pH > 7 and, finally, within the methacrylic ester copolymer Eudragit® RS100 which is pH independent and slowly erodes and releases its contained cargo. The antibacterial action of those advanced wound dressings has been evaluated against methicillin-sensitive *S. aureus* Newman strain expressing the coral green fluorescent protein (cGFP), as a model of a Gram-positive bacteria, and against *E. coli* S17 strain as a model of a Gram-negative bacteria. It was demonstrated that those combinational products integrate in one device the required characteristics for a wound dressing with the therapeutic action of a contained active principle and can be selected depending on the wound acidic or alkaline status for its appropriated management.

1. Introduction

Wound healing involves a cascade of physiological processes that rapidly activate to alleviate the infringed damage, promoting homeostasis, inducing coagulation, inflammation, cell proliferation, migration and regeneration, wound remodeling, and scar tissue formation (Velnar et al., 2009). This process may be delayed, incomplete and disturbed when skin infection occurs, producing complicated or even chronic non-healing wounds. When skin structure and function are not restored in a timely manner, the original acute wound is defined as chronic (e.g., venous, pressure, diabetic, and arterial insufficiency ulcers) being those wounds usually promoted by preexisting pathophysiological conditions. In those chronic wounds, the standard treatment is not enough to restore skin function and regrettably chronicity remains within the wound showing inflammation, hyperproliferative tissue, and having a permanent non-advancing wound edge.

A polymicrobial dynamic biota is responsible for wound infection. The origin of those facultative microorganisms can be the environment, the host microbiota around the wound and other endogenous sources involving mucosal membranes (i.e., gastrointestinal, oropharyngeal, and genitourinary mucosae) (Bowler et al., 2001). There are several challenges when treating chronic non-healing wounds including the selection of the appropriate antimicrobial treatment depending on the culture results, because of the dynamic and complex aerobic and

* Corresponding authors at: Instituto de Nanociencia y Materiales de Aragón (INMA), CSIC-Universidad de Zaragoza, Zaragoza 50009, Spain.
E-mail addresses: arruebom@unizar.es (M. Arruebo), sirusta@unizar.es (S. Irusta).

https://doi.org/10.1016/j.ijpharm.2022.122003
Received 8 April 2022; Received in revised form 13 June 2022; Accepted 5 July 2022
Available online 8 July 2022

anaerobic polymicrobial biota, composed of fungi and bacteria (Kalan and Grice, 2018) and because most of the bacteria remain still nowadays unculturable by current microbiological techniques (Schloss and Handelsman, 2004). In addition, bacterial biofilm (i.e., dynamic aggregated populations of bacteria embedded in a self-secreted extracellular polymeric substance named glycocalyx which is composed of polysaccharides, polypeptides and DNA) is present in 60–90% of chronic wounds (Attinger and Wolcott, 2012; Kadam et al., 2019) making antimicrobial regimens unsuccessful due to antimicrobial shielding and due to a reduced metabolic activity of bacteria after changing its phenotype when organized as biofilms.

Most of chronic wounds are treated with topical antiseptics such as octenidine dihydrochloride, polyhexanide, iodophors, chlorhexidine, silver-sulfadiazine, and combinations thereof. The main advantages of common antiseptics are their limited potential to contribute to the development of bacterial resistance or cross-resistance due to their multiple non-specific mechanisms of antimicrobial action, their broad spectrum activity, their easy permeation through necrotic tissue, eschar, and bacterial biofilms, and their low cost (Bigliardi et al., 2017). However, some of them also show large limitations in the management of chronic wounds such as cytotoxicity against eukaryotic cells rendering delayed wound closure, environmental persistence and accumulation, genotoxicity at high doses, etc. (ECHA, 2011; Kramer et al., 2018). Last but not least, topical antibiotics are also used on chronic wounds when an increased bioburden is observed, cellulitis, compromised host defenses or risks of bacteremia (Roberts et al., 2017); however, antibiotic resistance remains as a major challenge for mankind. Many topical antibiotics have rapidly promoted the development of resistance including mupirocin, clindamycin, polymyxin, neomycin, fusidic acid, etc. (Roberts et al., 2017).

All in all, a successful management of chronic infected wounds remains as an unmet need for the healthcare sector. Numerous reports have quantified the direct and indirect costs associated with chronic non-healing infected wounds and all of them warn that population aging and comorbid growing illnesses, such as diabetes, are concerns which might further increase the tremendous social and health care burden (Olsson et al., 2019). For instance, in Europe, there are more than 60 million patients suffering from diabetes, of those between 19% and 34% are vulnerable to developing a diabetic foot ulcer during their lifetime and approximately 20% of moderate or severe diabetic foot infections result in lower extremity amputations (Edmonds et al., 2021). Almost 33% of patients with spinal cord injury develop pressure ulcers revealing again an inadequate prevention of chronic pressure wounds (Shiferaw et al., 2020).

Timing plays a role when treating infected wounds because after bacterial colonization released cytokines and metalloproteinases prolong the inflammatory stage and induce extracellular matrix (i.e., collagen, elastin, fibrin, etc.) degradation, respectively, delaying healing (McCarty and Percival, 2013). Chronic wounds are characterized by an alkaline pH compared to the neutral pH of acute wounds or to the acidic pH of intact skin (Jones et al., 2015). Consequently, it would be interesting to develop medicated wound dressings with pH-responsiveness and also having burst or delayed release of antimicrobials for the management of chronic non-healing wounds to match antimicrobial release to the different bacterial growth kinetics on the wound bed. Herein, we have developed antimicrobial wound dressings loaded with antiseptics (i.e., chlorhexidine), broad-spectrum antibiotics (i.e., rifampicin) and with the antimicrobial of natural origin thymol within pH-dependent methacrylic acid copolymers (Eudragit® L100-55) which dissolve at pH $>$ 5.5; also within Eudragit® S100, which dissolves at pH $>$ 7 and, finally, within methacrylic ester copolymers (Eudragit® RS100) which are pH independent and slowly erode and release their contained cargo. The objective is to finely tune the antimicrobial release kinetics depending on the needs and to the wound specific pH in a timely manner.

2. Materials and methods

2.1. Materials

Eudragit® L100-55 (L100-55), Eudragit® S100 (S100) and Eudragit® RS100 (RS100) were generously donated by Evonik Industries AG (Essen, Germany). Chloroform ($CHCl_3$,anhydrous, $\geq$99%), N,N-Dimethylformamide (DMF, $>$99%), dimethyl sulfoxide (DMSO, $>$99%), Tween® 80, phosphate-buffered saline (PBS), tris(hydroxymethyl)aminomethane (Tris), rifampicin (RIF, $\geq$97%), chlorhexidine (CHXD, $\geq$99.5%) and thymol (THY, $>$98.5%) were purchased from Sigma-Aldrich (Darmstadt, Germany). Ethanol absolute (EtOH) was purchased from Panreac AppliChem (Barcelona, Spain). All reagents were used as received without any further purification. Tryptone soy broth (TSB) and tryptone soy agar (TSA) were purchased from Laboratorios Conda-Pronadisa SA (Madrid, Spain). GFP-expressing antibiotic-sensitive *Staphylococcus aureus* was kindly donated by Dr. Cristina Prat, Institut d'Investigació en Ciencies de la Salut Germans Trias i Pujol (IGTP, Spain) and *Escherichia Coli* S17 was kindly donated by Dr. Jose A. Ainsa, University of Zaragoza (Zaragoza, Spain). High-glucose Dulbecco's modified Eagle's medium (DMEM; DMEM w/stable glutamine) and antibiotic − antimycotic (60 μg/mL penicillin, 100 μg/mL streptomycin, and 0.25 μg/mL amphotericin B) were supplied by Biowest (Nuaille, France). The medium was supplemented with 10% (v/v) fetal bovine serum (FBS) from Gibco (Thermo Fisher Scientific, Waltham, Massachusetts, USA). The Blue® cell viability assay, used to evaluate potential cytotoxicity, was purchased from Abnova (Abnova GmbH, Taipei, Taiwan).

2.2. Synthesis of pristine and medicated electrospun fibers and characterization

2.2.1. Synthesis of pristine and medicated fibers

L100-55 and S100 solutions (30% w/v) were prepared by dissolving the corresponding polymers in a DMF:EtOH (4:1) mixture that was stirred overnight at 600 rpm at room temperature (27 °C). RS100 solution (30% w/v) was prepared in $CHCl_3$. For the synthesis of RIF, CHXD and THY loaded fibers, the adequate amount of the therapeutic agent (2.5%, 5% and 20% w/w, respectively, referred to the polymer weight) was added to the different L100-55, S100 and RS100 solutions and then mixed for 30 min. Fibers of the three polymers loaded with each one of the bactericidal agents selected were prepared.

Each of the resulting solutions were loaded in 10 mL syringes that were then connected to an Yflow 2.2 D500 electrospinner (Electrospinning Machines/R&D Microencapsulation, Spain) equipped with a flat plate collector covered with aluminum foil. For all the solutions the flow rate was set at 1.0 mL/h, and the distance between the tip of the needle and the collector was fixed at 18.5 cm when electrospinning L100-55 and at 15 cm for S100 and RS100. To produce plain and RIF-loaded RS100 fibers it was necessary to use a coaxial needle feeding chloroform through the outer needle to avoid plugging whereas the drug dissolved in the polymer flowed through the inner needle. The negative voltage applied in all cases was set in the range –2 to −4 kV and the positive one applied to the needles varied from + 7.69 to + 15.07 kV. This voltage was adjusted in each case until reaching a stable Taylor cone during the electrospinning process. The production process was carried out at room temperature (27 °C) with a relative humidity of 30–50%. The viscosity of the solutions (before the electrospinning process) was determined by means of a FUNGILAB V.1.0 VISCO BASIC viscometer (8 μL adapter/30 rpm/20 °C).

2.2.2. Morphology characterization

The morphology of the obtained fibers was analyzed by scanning electron microscopy (SEM). Samples were sputtered with a Pd layer before observation and images were acquired with an Inspect F50 FEG scanning electron microscope (FEI company, USA). Nanofiber diameters

were measured (N = 200) using the DigitalMicrograph® software (Version 2.31.734.0).

2.2.3. Effect of pH

The effect of the pH on the resulting fibers was first studied by introducing the fibers in buffers at different pHs (5.5, 7.4 and 8.2) for 1 h, dried for 12 h, and then analyzing their resulting morphology by SEM. But since for L100-55 polymers the fibers were completely dissolved after immersing them in pH 7.4 and 8.2 buffers, the test was carried out just by depositing 10 μL of this buffer on the surface of several electrospun membranes.

2.2.4. Antibacterial agents load

RIF, CHXD and THY loadings in the fibers were measured by UV − vis spectrophotometry (Jasco V670, Jasco Applied Science, Eschborn, Germany) at a wavelength of 340 nm, 254 nm and 276 nm, respectively by dissolving 2 mg of the drug-loaded fibers in 1 mL of DMSO. A baseline of the same amount of each dissolved non-loaded polymer was subtracted to eliminate any potential interference. The encapsulation efficiency (EE) and the drug loading (DL) were calculated with Eqs. (1) and (2), respectively:

$$EE(\%) = \frac{mass\ of\ entrapped\ drug(mg)}{mass\ of\ drug\ added(mg)} \times 100 \quad (1)$$

$$DL(\%) = \frac{mass\ of\ entrapped\ drug(mg)}{Total\ mass\ of\ drug\ loaded\ nanofibers(mg)} \times 100 \quad (2)$$

Fourier-transform infrared (FTIR) spectra were recorded to evaluate drug − polymer molecular interactions using a Bruker VERTEX 70 FTIR spectrometer (Bruker, Billerica, MA, USA) equipped with a Golden Gate diamond ATR accessory. Spectra were recorded by averaging 40 scans in the 4000–600 cm^{-1} wavenumber range at a resolution of 4 cm^{-1}.

Raman measurements were carried out using a confocal benchtop WITec Alpha 300 (spectral resolution 2 cm^{-1}) with an excitation wavelength of 785 nm and with a laser power of 30 mW for the fibers with RIF and with an excitation wavelength of 633 nm with a laser power of 10 mW for fibers loaded with CHXD and THY; all measurements were made in backscattering configuration.

2.2.5. In vitro drug release

For the evaluation of drug release kinetics, different pH buffered solutions (pH = 5.5, 7.4 and 8.2) were tested to emulate the different pH values of a wound, using a J.P. Selecta Movil-Rod rotating shaker at 37 °C under sink conditions: a solution at pH 5.5 based on sodium acetate 2.05 g + acetic acid 1.5 mL + NaOH 2 N was used to mimic intact skin pH, a solution at pH 7.4 based on 0.1 M PBS was used to mimic the wound healing phase in which cellular proliferation and granulation take place and a solution at pH 8.2 based on 0.1 M TRIS solution was used to mimic infected wounds pH. 5 mg of fibers of each drug loaded polymer with every pharmaceutical agent were immersed in 5 mL of each different buffered solution (pH = 5.5, 7.4 and 8.2) during 24 h under stirring (60 rpm). When using RS100 samples 2% of Tween® 80 was added promote drug release due to their high hydrophobic nature. At predetermined time intervals, 1 mL of the supernatant was collected by centrifugation for 1 min at 3000 rpm and an equal volume of fresh solution was replenished. Four different samples were independently analyzed by UV − vis spectrophotometry (Jasco V670, Jasco Applied Science, Eschborn, Germany) subtracting the base line obtained for each non-loaded polymer. The release kinetics were determined by fitting the experimental data with different release kinetics models.

2.3. In vitro biological analyses

2.3.1. Antibacterial activity assay

To evaluate the antibacterial activity of free RIF and THY both compounds were evaluated against methicillin-sensitive *S. aureus* Newman strain expressing the coral green fluorescent protein (cGFP), as a model of a Gram-positive bacteria, and against *E. coli* S17 strain as a model of a Gram-negative bacteria. Both microorganisms were grown overnight in TSB at 37 °C under continuous shaking (150 rpm) until reaching the stationary growth phase (10^9 colony forming units (CFU/mL), afterwards they were diluted in TSB until reaching 10^5 CFU/mL. The inoculum was placed into tubes containing a specific quantity of RIF (0–1 ppm for *S. aureus* and 0–60 ppm for *E. coli*) and THY (20–250 ppm for both bacteria) dissolved in 2% DMSO (which previously demonstrated no bactericidal action at that concentration). After 24 h at 37 °C and 150 rpm of incubation stirring rate, the standard serial dilution method was used to determine viable bacteria. As positive controls, untreated *S. aureus* GFP and *E. coli* S17 were included and, also an assay using only 2% DMSO (without the antimicrobials agents) on the selected bacteria was performed to corroborate that that concentration did not exert any antimicrobial action.

Minimal inhibitory concentration (MIC) and minimum bactericidal concentration (MBC) for RIF and THY loaded electrospun membranes were tested according to the ASTM E-2180–18 standard test method (Koester, 2018). Membranes were cut and placed in 24-well plates after sterilization under UV light (30 min for each side). For that end, 60 mL of warm TSA (47 °C) was inoculated with 10^5 CFU/mL of the selected bacteria. Then, each well of the plate containing the membranes were filled with 2 mL of the inoculated TSA and incubated in a closed box with water (to keep an adequate humidity and avoid desiccation) at 37 °C for 24 h. When using RS100 samples 2% of Tween® 80 was added to the inoculated TSA due to its high hydrophobic nature in order to be able to promote drug release. Tween® 80 was not used when measuring drug release from L100-55 and S100 polymers due to their larger hydrophilicity. Afterwards, each sample was transferred to a Falcon type flask, and 18 mL of TSB were added. Each sample was sonicated for 15 min and vortexed for 1 min to detach bacteria. The standard microdilution method was used to determine viable bacteria. A positive control was also included and each experiment was performed in triplicate.

The fibers loaded with CHXD were also tested against *S. aureus* Newman GFP and *E. coli* S17 but using the Antimicrobial Disk Susceptibility Tests as described in the US Clinical and Laboratory Standards Institute (CLSI) since with the test previously used for RIF and THY, the drug apparently did not diffuse properly to reach all the agar within the well and large heterogeneity was observed compared to the results showed by the free drug. This phenomenon was not observed for RIF or THY probably due to the high volatile nature of the THY, which made possible to reach all the well and dissolve from the vapor phase into the solid agar and due to the high antimicrobial efficacy of the RIF. Therefore, to test the CHXD loaded Eudragit-based membranes, disks of different diameters (12, 16 and 20 mm) were cut and sterilized under UV light (30 min on each side). Agar petri dishes were inoculated with 300 μL of a suspension of each bacteria (*S. aureus* GFP *and E. coli*) at 10^7 CFU/mL. Fibers were placed in the inoculated petri dishes (3 samples per dish) and after overnight incubation at 37 °C the zone of inhibition (area of no growth) was measured using a caliper.

2.3.2. Cytotoxicity

To determine the cytocompatibility of the synthesized fibers, J774 macrophages were used to evaluate the potential cytotoxic effects of L100-55, S100 and RS100-RIF/CHXD/THY-loaded fibers. Macrophages were grown in DMEM containing 2 mM L-glutamine supplemented with 10% (v/v) FBS and 1% (w/v) antibiotic–antimycotic, incubated in a humidified atmosphere at 37 °C and 5% CO_2. Cytotoxicity was measured using the Blue® cell viability assay (Abnova, Taiwan) according to the manufacturer's instructions. Cells were seeded in 24-well plates (34,000 cells per well), and 4 mg/mL of L100-55, S100 and RS10O-RIF/CHXD/THY were added to the cultures (2 mL) and free drugs were added at 40 μg/mL (RIF), 8 μg/mL (CHXD) and 250 μg/mL (THY) according to the highest value of each MBC obtained for the drug-loaded fibers. Samples were incubated at 37 °C, 5% CO_2 for 24 h. Later, membranes were

removed, and cells were washed twice with PBS. Then, cells were incubated with the Blue® cell reagent (10% (v/v) in supplemented DMEM) and incubated for 4 h at 37 °C and 5% CO_2. Fluorescence was measured at 530/590 nm excitation/emission wavelengths in a Multimode Synergy HT microplate reader (Biotek, WI, USA). Cell viability was determined by comparing the values retrieved for the treated cells and for untreated controls which were assigned with 100% viability. Each determination was performed in triplicate having four replicas in each experiment, using independent syntheses.

2.4. Statistical analysis

All results are expressed as mean ± standard deviation (SD). Two-way analysis of variance (ANOVA) was used to analyze cellular experiments (GraphPad Prism 9, San Diego, USA). Statistically differences were considered when $p \leq 0.05$.

3. Results and discussion

3.1. Fibers morphological characterization

The morphology of drug loaded and un-loaded Eudragit based fibers was studied by SEM, results are shown in Fig. 1. Solutions of all polymers with a concentration of 30% w/v showed adequate spinnability; however, the drug loading depends on the nature of the antibacterial compound present. While only 2.5 w/w % of RIF could be added to the polymer solution in order to obtain a stable Taylor cone during electrospinning, 5 w/w % of CHXD and a content as high as 20 w/w % of THY could be added to the corresponding organic polymeric solutions and getting defect free electrospun fibers (i.e., homogeneous diameters and beads free) after optimizing the fabrication conditions. During this initial optimization process the incorporation of the maximum amount

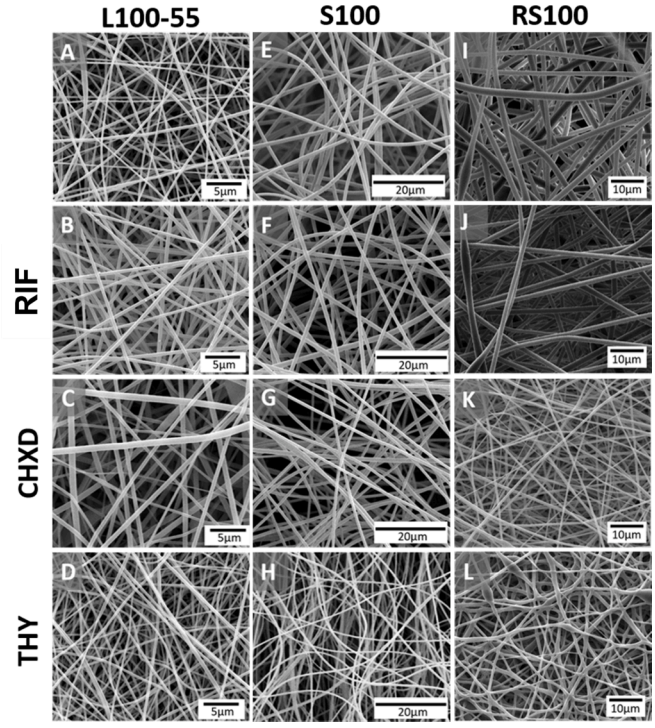

Fig. 1. SEM images of: (A) L100-55, (B) L100-55/RIF, (C) L100-55/CHXD, (D) L100-55/THY, (E) S100, (F) S100/RIF, (G) S100/CHXD, (H) S100/THY, (I) RS100, (J) RS100/RIF, (K) RS100/CHXD, (L) RS100/THY. RIF, THY and CHXD stand for rifampicin, thymol and chlorhexidine, respectively. The morphology of each polymeric electrospun fibers with and without the corresponding antimicrobial compounds is shown.

of the antimicrobial compound in the electrospinning solution was tried while maintaining a stable Taylor cone. There was an important difference in the resulting polymer-based fiber diameters, while L100-55 fibers had 324 ± 77 nm in diameter, the mean diameter for S100-based electrospun fibers was 1167 ± 2246 nm and for RS100 it increased to 1751 ± 395 nm (Fig. 1, Table 1). The important difference between L100-55 and S100 fibers diameters would be attributed to the different viscosity of the initial electrospinning solutions (Table 1) because it is known that the increase in viscosity results in larger fiber diameters (Reda et al., 2017). As the viscosity increases, the viscoelastic forces became the dominant factor producing fibers with larger diameters. As was mentioned before, the high volatility of chloroform required the use of a coaxial needle feeding only solvent in the outer needle to avoid clogging. The use of a different solvent and a coaxial needle completely changes the electrospinning conditions and the obtained fibers had larger diameters. Also, the solution conductivity strongly influences the electrospinning process, as the solution conductivity increases, the fiber diameter decreases and vice versa (Ibrahim and Klingner, 2020). The lower conductivity of the solvent chloroform compared to that of DMF:EtOH would explain the larger fiber diameters obtained for RS100 fibers.

The addition of the antimicrobials to L100-55 slightly modified the solution viscosity and the voltage required, and as a consequence, the obtained fiber diameters were similar to those obtained for the non-loaded polymers. A different result was obtained with the addition of antimicrobials to S100-based electrospinning solutions. The increase in voltage required to produce a stable Taylor cone after the addition of the corresponding drugs produced an increase in the speed with which the polymer solution traveled from the needle to the collector resulting in larger fiber diameters, as corroborated in the previous literature (Meechaisue et al., 2006). The decrease in the voltage needed to produce homogeneous RIF loaded S100 fibers from 20.3 to 14.2 KV would be the reason for the lower diameter obtained in this case. The effect of applied voltage could also be noticed for CHXD and THY S100 loaded fibers. Viscosity seems to be the ruling parameter for directing RS100 fiber morphology since fiber diameter decreases with the addition of CHXD and increases for THY loaded fibers. It is important to point out that THY loaded RS100 fibers were very fragile and brittle and they collapsed when collecting them from the aluminum foil.

3.2. Bactericidal agent encapsulation

Even when the concentration of RIF in the electrospinning solutions was very low, the encapsulation efficiency (EE) was always higher than 90%. High EEs, higher than 75% were also previously found for RIF encapsulated in poly(lactic-co-glycolic acid) (PLGA) by electrospinning, attributed to the strong supramolecular interactions between RIF and this polymer (Gilchrist et al., 2013). On the other hand, the EE of CHXD was around 32% for all polymers and as consequence the drug loading never exceeded 1.6% w/w. For THY the EE depends on the encapsulating polymer and it was as high as 64.3% for S100 and as low as 16% for L100-55, while for RS100 it was 31%.

The different EE for the three drugs for each polymer could be related to their different physical properties. The negligible vapor pressure of RIF could lead to the high loading efficiency found for this drug, since its loss during the evaporation of the solvent in the electrospinning process would be negligible. CHXD has higher vapor pressure ($2 \cdot 10^{-14}$ mm Hg at 25 °C), although still very low, but the drug could partially evaporate during fiber formation resulting in a lower EE. THY is highly volatile and the higher distance between the tip and the collector used in this case (18.5 cm) could also explain the lower EE in L100-55 fibers compared to S100 and to RS100 fibers. However, this would not be the only factor affecting the loading because using the same tip to collector distance (15 cm), EE for S100 doubled the one obtained for RS100. The different solvents used to obtain the electrospinning solutions could be the factor affecting those loading efficiencies. The low viscosity of RS100 in the

Table 1
Fibers average diameter (N = 200), bactericidal encapsulation loading and encapsulation efficiency.

	Antimicrobial agent	Diameter (nm)	Total voltage (KV)	Viscosity (mPa.s)	Drug loading (% w/w)[a]	Encapsulation efficiency (%)
L100-55	–	324 ± 77	17.6	643	–	–
	RIF	450 ± 97	17.8	645	2.1	95 ± 7
	CHXD	317 ± 98	15.7	680	1.6	34 ± 3
	THY	302 ± 78	17.1	632	2.8	16 ± 2
S100	–	1167 ± 246	20.3	937	–	–
	RIF	536 ± 82	14.2	936	2.3	94 ± 5
	CHXD	854 ± 110	18.3	956	1.5	32 ± 2
	THY	656 ± 93	17.8	940	11.0	64 ± 3
RS100	–	1751 ± 395	14.7	125	–	–
	RIF	1762 ± 391	9.8	128	2.2	90 ± 2
	CHXD	1171 ± 272	16.5	105	1.5	31 ± 2
	THY	1857 ± 362	11.2	153	5.2	31 ± 8

[a] relative to the polymer weight.

chloroform solution would probably allow a higher migration of THY to the fibers surface and the consequent loss of the drug as previously reported for similar systems (Obeidat and Price, 2003).

The presence of the antimicrobial agents in the fibers as well as the possible interaction between polymers and compounds were analyzed by FTIR (Fig. 2). The presence of RIF in the L100-55 fibers could be confirmed by the band at 1240 cm^{-1} in the spectrum retrieved from the loaded fibers that would be attributed to the C-O-C vibrations in RIF (Zeng et al., 2021). Besides that, there were shifts in the region characteristic of the bands related to the C═O stretching for the polymer. The intensity of the band assigned to the carboxylic acid groups (1703 cm^{-1}) decreased compared to the C═O stretching band due to the esterified carboxylic groups (1726 cm^{-1}) suggesting acid-base interactions between L100-55 and RIF as previously reported (Liu et al., 2018). In the CHXD-loaded fibers spectrum, the bands at 1530 and 1492 cm^{-1} could be attributed to NH bending vibrations of the secondary amines and imine groups (Al-Ani et al., 2019). This last band appeared at 1485 cm^{-1} in the CHXD spectrum, the shift would indicate some supramolecular interactions between the polymer and the NH groups of the drug. The presence of THY in the THY-loaded L100-55 spectrum was shown by the appearance of a weak band at 942 cm^{-1} related to ═CH out-of-plane bending adsorption (Lukic et al., 2020).

No signals of RIF could be seen in S100 loaded fibers, even considering that the antimicrobial content in those fibers was similar to the one in L100-55 fibers, probably because the main peak of RIF at 1240 cm^{-1} overlaps with the signal of the polymer at 1239 cm^{-1} attributed to the C-C-NH^{+} bending of the amine group (Liu et al., 2018). On the other hand, bands at 1532 and 1577 cm^{-1} that appear in CHXD-loaded fibers could be related to the NH bending vibrations of secondary amines and imine groups (Holešová et al., 2015). The shift of these bands would indicate an interaction between the drug and the polymeric matrix. Several bands related to THY can be seen in THY-loaded S100 fibers confirming the presence of the drug. There was also an overlapping of bands for RIF-loaded RS100 fibers, hindering the observation of the bands related to

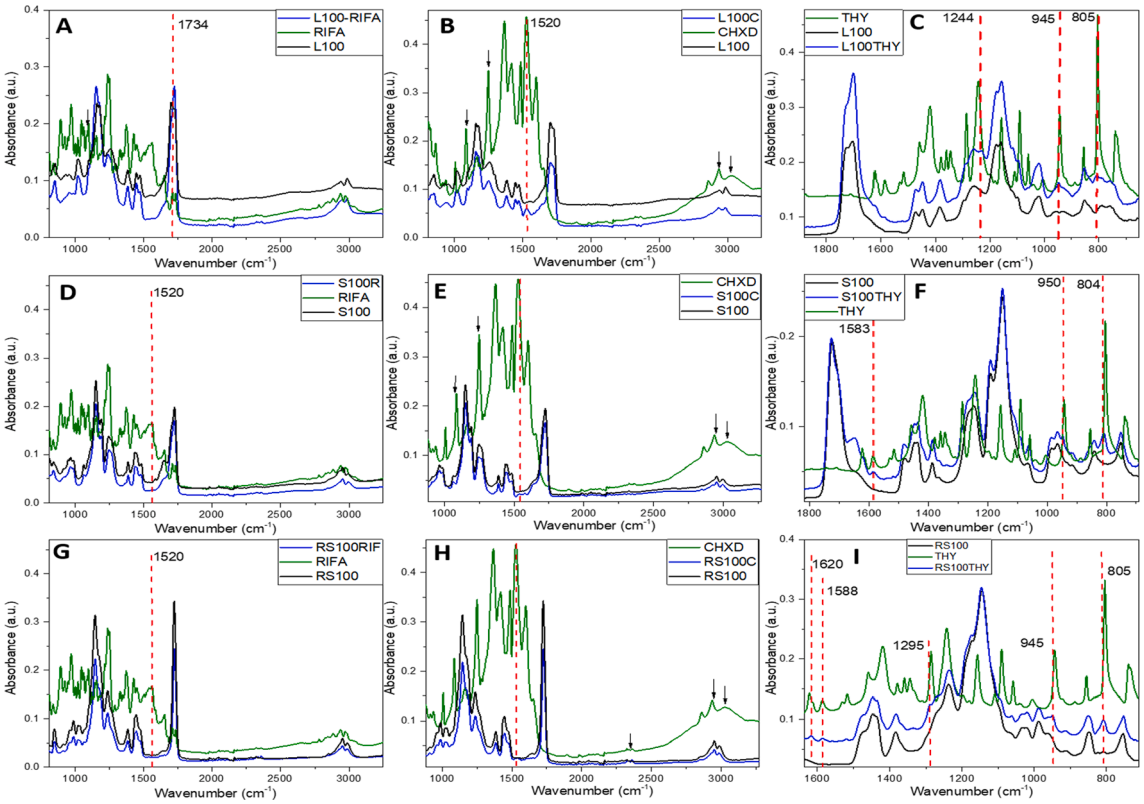

Fig. 2. FTIR spectra of loaded and unloaded fibers, (A), (B) and (C) L100 fibers; (D), (E) and (F) S100 fibers; (G), (H) and (I) RS100 fibers.

the antimicrobial presence in the loaded fibers. The band at 1531 cm^{-1} caused by the NH bending vibration in CHXD could be observed in the loaded fibers and again bands attributed to THY appeared in THY-loaded RS100 fibers. It is important to notice that in all THY-loaded spectra there were evident shifts of the bands attributed to the antimicrobial suggesting strong supramolecular interactions between THY and the host polymers.

Raman spectra of drug-loaded and non-loaded L100-55, S100 and RS100 are shown in Fig. 3. Bands at 1331 and 1570 cm^{-1} assigned to C—C stretching vibrations in RIF molecules could be observed in the L100-55 and S100 loaded fibers. In RS100 fibers, a band at 1340 cm^{-1}, assigned to normal modes with contributions of C—C, C—N and C—O stretching vibrations confirmed the presence of RIF in the fibers (Filgueiras et al., 2016).

In CHXD-loaded L100-55 and S100 the characteristic CHXD band at 1604 cm^{-1} was observed. This band is shifted compared to that of pure CHXD suggesting an interaction of the antiseptic with the host polymer (Chen et al., 2008). The band observed at 1294 cm^{-1} in the loaded fiber spectrum was also related to the CHXD molecule (Xia et al., 2014). Vibration normal mode at 1604 cm^{-1} present in the CHXD spectrum corresponded to chlorophenyl groups (Suci et al., 2001), while in the RS100-CHXD these vibrations were not found. That result could suggest that the entanglement of the polymer chains of RS100 does not allow the drug to have the vibrations that the free molecule would present.

The Raman mode at 740 cm^{-1}, characteristic of THY molecules and assigned to a combined motion from CC (ring) stretching and CCC (ring) bending could be observed in S100 and RS100 loaded fibers spectra, but in the spectrum corresponding to THY-loaded L100-55 that mode overlaps with the peak at 755 cm^{-1} which is associated to the CC vibrations of the polymer (Martín-Illana et al., 2021). However, the peak at 1270 cm^{-1} assigned to the combination of the C—C and C—O stretching as well as the HCC bending and the peak at 1622 cm^{-1} related to C-C ring stretching of THY all confirm the presence of the antimicrobial compound in the loaded fibers (Saraiva et al., 2020).

3.3. Effect of pH in fibers morphology

The effect of different pHs (5.5, 7.4 and 8.2) on the morphology of the fibers was analyzed by SEM (Fig. 4). As expected, the pH responsive character of L100-55 polymer was confirmed being affected even at pH 5.5, under those conditions fibers lost their cylindrical shape and diameters decreased. As expected,(Patra et al., 2017) drops of buffer at pH 7.4 on the electrospun mats produced the fusion of the fibers and they were almost completely fused at pH 8.2. On the other hand, even though the S100 polymer is reported to be soluble at pH > 7, fibers did not seem to be affected at pH 7.4, probably because the deposition of a few buffer drops on the mats was not enough to carry out the complete deprotonation of their carboxylic groups, but at pH 8.2, the fibers started to lose their cylindrical shape. RS100, is a pH-independent polymer and as a consequence, fibers did not suffer any morphological change after being exposed to pH 5.5, 7.4 and 8.2, even when in this case, the membranes were complete immersed in the corresponding buffers. Probably longer immersion times would be needed to observe matrix erosion.

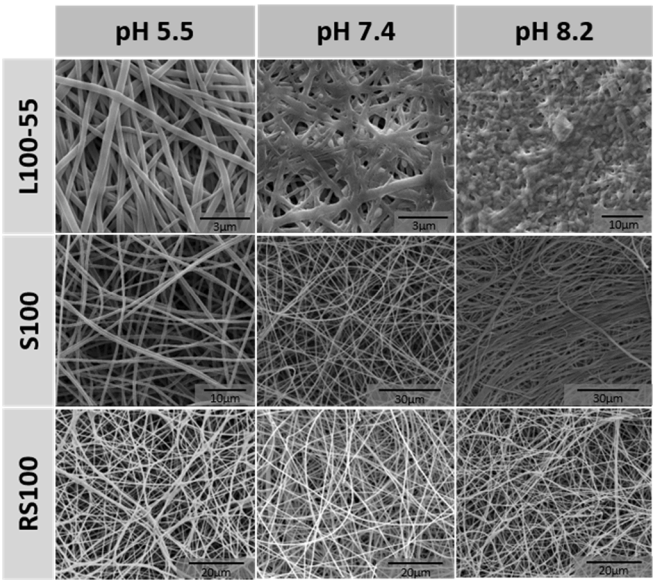

Fig. 4. Effect of pH in the polymer fibers morphology.

3.4. Antimicrobial agents release

RIF was completely released from the L100-55 polymer at any pH, even though FTIR results suggested acid-base interactions between the

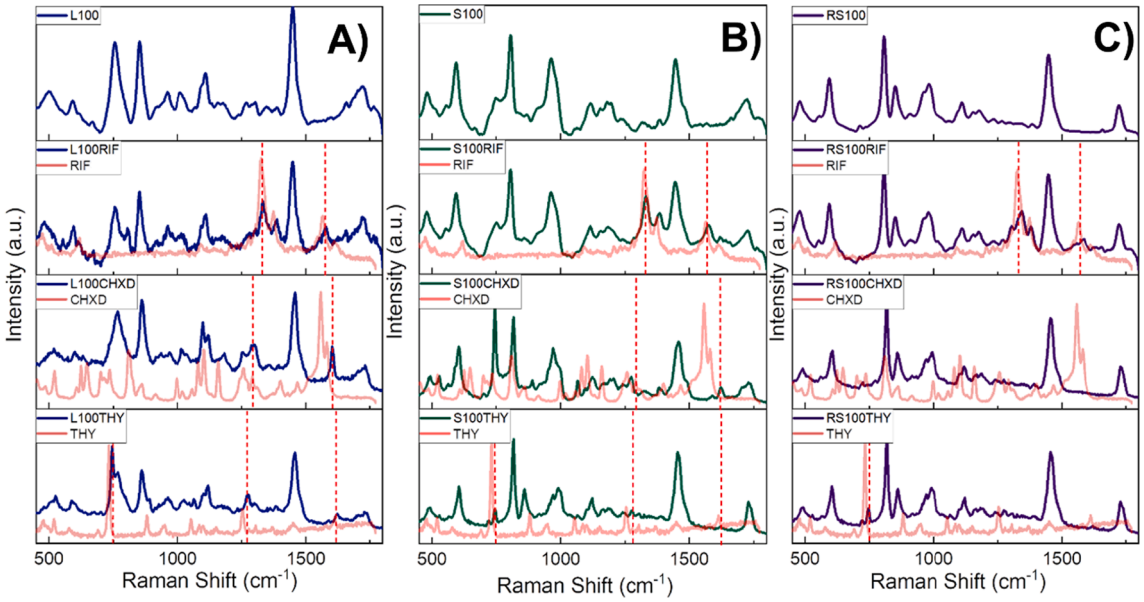

Fig. 3. Raman spectra of unloaded and loaded (A) L100-55 fibers; (B) S100 fibers and (C) RS100 fibers.

drug and the polymer, the dissolution of the polymer would trigger the complete release of all loaded RIF after 24 h (Table 2). The same behavior could be observed for S100-based polymeric fibers, at pH 7.4, when the fibers started to be affected by the pH, RIF release reached 100%, while in an acidic buffer only 25% of loaded RIF was released after 24 h. On the other hand, release from RS100 fibers was not dependent on the pH, because, as was mentioned before, this polymer does not solubilize at any pH.

The release of CHXD from L100-55 fibers was promoted with an increased pH reaching 100% release at pH 8.2. In this case, the interaction between the polymer and the N-H groups of the drug would avoid the complete burst release at lower pHs attributed to a lower dissolution degree. CHXD release from S100 fibers presented a completely different behavior, there was the expected release increase when the pH changed from 5.5 to 7.4, but further pH increase to 8.2 led to a decrease in the amount of released drug. This effect could be related to an ionization of the released CHXD at the pH of the dissolution medium, higher than the CHXD pKa, that causes its re-adsorption on the fibers surface as previously reported for other drugs (Pignatello et al., 2001). Furthermore, during the S100 dissolution process, due to the weakening of the hydrogen bonding between the polymeric chains, more carboxylic groups could become accessible to interact with the cationic CHXD molecules (Giménez-Martín et al., 2009). CHXD cumulative release from RS100 fibers reached 88% at pHs $>$ 7.4, while at pH 5.5 the release was 64%.

THY, as RIF, was completely released from L100-55 due to the dissolution of the polymer after 24 h in solution. However, the release of THY from S100 fibers slowly increased with the pH, and only 43.6% of the drug was released at the highest pH. This behavior could be due to the supramolecular interactions between THY and the S100 polymer as suggested by the FTIR results. As was mentioned before, THY loaded RS100 fibers were too brittle to evaluate the drug release for that reason those were discarder for further studies.

Skin surface pH ranges between 5.4 and 5.9 but it gradually increases with depth. This might explain the rather higher pH values, close to neutrality, found immediately after the skin integrity destruction in an acute wound (Taeger et al., 2021). During healing and reestablishing the intact stratum corneum, the wound, as scar tissue returns to an acidic pH (Haller et al., 2021). On the other hand, in chronic wounds the pH values vary in the range 5.45–8.65, due to the so-called alkaline shift (Wiegand et al., 2015). Wound alkalinity would be caused by dissolved CO_2, a reduction in oxygen tension and, possibly, by alkaline anions accumulation from bacterial metabolism. It was postulated that the different pH values found in wounds require different drug-loaded dressings having pH-responsiveness loaded with antiseptics and antibiotics exerting different release kinetics in order to have a perfect match between the drug release kinetics and the conditions of each wound type.

In this scenario, different antimicrobial-loaded electrospun membranes were developed to potentially be used as wound dressings in order to grant a successful management of infected wounds. As was mentioned before, chronic wounds are characterized by an alkaline pH compared to the neutral pH of acute wounds or to the acidic pH of intact skin (Jones et al., 2015). Therefore, according to the release kinetics observed (Table 2) in the prophylaxis against infection development on intact skin at a pH of 5.5 RIF loaded-L100-55 composing dressings would release the loaded antibiotic immediately eliminating any potential pathogenic bacteria present from colonizing the wound. In the management of infected chronic wounds (i.e., having alkaline pH) CHXD-loaded L100-55 composing dressings would be recommended because they would release the antiseptic over time reaching a maximum under alkaline conditions (Table 2). Finally, in the management of acute wounds (i.e., having neutral pH) RIF-loaded S100 composing fibers would be recommended showing a sustained release reaching a maximum under neutral pH (Table 2).

Table 2
Antimicrobial agents release kinetics after 24 h in buffers at different pHs.

Polymer	Antimicrobial agent	Drug released at 24 h (%)		
		pH 5.5	pH 7.4	pH 8.2
L100-55	RIF	100 ± 0.5	100 ± 2	100 ± 3
	CHXD	13 ± 2	40 ± 5	100 ± 4
	THY	100 ± 15	100 ± 10	100 ± 16
S100	RIF	25 ± 5	100 ± 2	100 ± 5
	CHXD	30 ± 3	72 ± 7	34 ± 9
	THY	30 ± 6	35 ± 1.7	43.6 ± 3.1
RS100	RIF	55 ± 0.2	49 ± 0.2	69 ± 0.2
	CHXD	64 ± 2	88 ± 8	100 ± 7
	THY	–	–	–

3.5. Antibacterial activity

The antibacterial activity of the three different free drugs studied was evaluated against *S. aureus* GFP and *E. coli* S17 to obtain the MICs and MBCs values to be compared later on with the ones obtained for the drug-loaded fibers (Table 3). To analyze the anti-pathogen response of drug-loaded fibers, a test was carried out where the fibers were immersed in 2 mL of agar inoculated with 10^5 CFU/mL of each pathogenic microorganism. The amount of the released drug from the corresponding drug-loaded dressing in PBS is also included in Table 3 to be used as reference to compare the dose of the drug released under optimal pH (7.4) conditions for bacterial growth due to the observed fast dissolution of drug-loaded fibers into the culture medium (i.e., agar).

In the case of RIF-loaded fibers against *S. aureus* GFP, 10–50 μg/mL of material were required to elicit bactericidal response, depending on the host polymer. Controls performed using non-loaded fibers showed that they do not have any antibacterial activity. Regarding to the total eradication of *S. aureus*, RS100 shows the best results based on the reduced amount of released RIF (1.07 μg/mL) compared with the released from L100-55 and S100 (2.10 μg/mL and 2.30 μg/mL, respectively). This effect can be attributed to the disintegration of RS100 fibers in the culture medium that leads to a burst release of RIF. On the other hand, compared to *S. aureus* higher quantities of the free drug are necessary against *E. coli S17* to elicit bactericidal action since RIF does not effectively penetrate the outer membrane of gram-negative bacteria (Drapeau et al., 2010). As in *S. aureus*, S100 loaded with RIF showed the best inhibitory activity against *E. coli*. In this line, our previous results concerning the use of polycaprolactone (PCL) nanofibers decorated with PLGA nanoparticles loading RIF also showed the same required range of released RIF (3–48 μg/mL) to achieve a significant reduction in bacteria growth being again necessary a higher RIF concentration to eradicate Gram negative vs Gram positive bacteria. Nevertheless, in the case of bactericidal activity against *E. coli*, L100-55 loaded with RIF shows the greatest action compared to the other polymers, because it requires the lowest drug loading (42 μg/mL) to achieve the highest levels of bacterial reduction. Although RIF loaded RS100 has antibacterial activity with an amount of drug released similar to that of S100 and L100-55, the required amount of fibers and drug released for exerting its inhibitory activity against *E. coli* were greater. This may be due to the fact that fibers of RS100 are pH independent, which means that even in contact with the culture medium they maintain their structure thus allowing a sustained drug release. For both bacteria, a larger amount of drug was required for eliciting inhibition and bactericidal action when loaded into the polymers compared to the action of the free drug because when RIF was embedded into the polymeric fibers, less drug immediately available for inhibiting RNA polymerase is present despite of the burst release observed for the pH-responsive polymers used. A similar effect has been reported by Gilchrist et al. (Gilchrist et al., 2013) who demonstrated that when RIF was embedded in PLGA nanofibers only concentrations able to reach the MIC were obtained and no bactericidal effect was observed.

Results from the antibacterial evaluation of THY-loaded fibers showed in Table 3 indicate the reduced concentration to elicit

Table 3
Antibacterial activity as Minimum Inhibitory Concentration (MIC) and Minimum bactericidal concentration (MBC) of free drugs and loaded fibers. RIF = Rifampicin; THY = Thymol.

Bacteria	Drug	Sample	MIC		MBC	
			Membrane concentration (μg/mL)	Drug released in 24 h (μg/mL)	Membrane concentration (μg/mL)	Drug released in 24 h (μg/mL)
***S. aureus* GFP**	RIF	Free	–	0.03	–	0.05
		L100-55	50	1.05	100	2.10
		S100	10	0.23	100	2.30
		RS100	50	0.53	100	1.06
	THY	Free	–	50	–	250
		L100-55	200	5.6	600	16.8
		S100	1000	38.5	1500	57.75
E. coli	RIF	Free		3	–	>12
		L100-55	250	5.25	2000	42.00
		S100	200	4.60	2000	46.00
		RS100	3000	32.34	>4000	>43.12
	THY	Free	–	80	–	200
		L100-55	500	14	1500	42
		S100	500	19.25	1000	38.5

antibacterial effects when using this antiseptic. As mentioned before, fibers made of RS100 loaded with THY could not be tested due to their brittle and fragile structure. However, fibers made of L100-55 and S100 showed large antimicrobial effect against both bacteria despite the low amount of THY released. Against *S. aureus*, compared to THY-loaded L100-55 fibers, increased amounts of THY-loaded S100 fibers were needed to obtain inhibitory (5 times more) and bactericidal activity (2.5 times more). On the other hand, L100-55, despite of the low amount of THY released, showed excellent inhibitory and bactericidal activity. Against *E. coli*, L100-55 loaded with THY is the most efficient system as inhibitor and bactericidal; however, the difference between this polymer and THY-loaded S100 is not as important as in the case of challenging it against *S. aureus*. Both systems show an improved antibacterial activity compared with the one shown by the free compound, suggesting that the combination and processing of THY with the used polymer creates an environment where the antibacterial effect of THY is largely enhanced. Although the application of nanofibers loaded with THY does not lower the pH of the medium to create an acidic environment, the dissolution of the fiber decreases the pH of the medium considerably. Juven et al. (Juven et al., 1994) showed that at low pH values, the THY molecule is undissociated, making the drug more hydrophobic producing a suitable environment for a better binding to the hydrophobic regions of the bacterial membrane and promoting the dissolution of the drug in the lipid region of the bacterial membrane. Previous studies in our group pointed to a superior antimicrobial efficacy of Eudragit®-based dressings compared to those based on electrospun PCL in which the inhibition of *S. aureus* and *E. coli* growth was achieved when THY was released at concentrations in the range of 70–220 μg/mL (Gámez et al., 2020; Gámez et al., 2019; Garcia-Salinas et al., 2020).

In the case of fibers loaded with CHXD, as mentioned before, the disk diffusion method was used due to limited drug diffusion compared to the one of the free drug to reach all the agar within the well. Other authors have previously demonstrated the importance of the direct contact to elicit bactericidal activity (Gámez-Herrera et al., 2020; Lessa et al., 2010; Luddin and Ahmed, 2013). Disks from CHDX-loaded fibers (12, 16 and 20 mm in diameter) were used to measure the inhibition zone against *S. aureus* and *E. coli* (Fig. 5). The average weight of each disk was ≈2 ± 0.15 mg for the 12 mm in diameter, ≈2.5 ± 0.1 mg for the 16 mm and ≈3.1 ± 0.11 mg for the 20 mm disks. Disks were left in contact for 24 h which means that the 12 mm L100-55 disks released 12 μg /mL of CHXD creating 15.2 ± 1.5 mm of inhibition against both *S. aureus* and *E. coli,* whereas the 20 mm in diameter disks releasing 16 μg/mL achieved a 21.6 ± 1.2 mm inhibition zone for both bacteria. In the case of S100 samples, 12 mm disks released 20 μg/mL creating an inhibition zone of 12.5 ± 0.8 mm against *S. aureus* and 14.6 ± 2 mm against *E. coli*. While the 16 mm disks extended to 17.3 ± 2.3 mm (*S. aureus*) and 18.5 ± 0.8 mm (*E. coli*) this inhibition zone; the 20 mm in diameter disks created an inhibition area of 21.6 ± 0.9 mm (*S. aureus*) and 23.7 ± 1.2 mm (*E. coli*), respectively. The RS100 disks, meanwhile, released 29 μg/mL (12 mm) creating 26 ± 2.1 mm inhibition zones against both pathogens, 33 μg/mL (16 mm in diameter) creating an inhibition zone of 24.4 ± 0.15 mm for *S. aureus* and 32.4 ± 0.5 mm for *E. coli* and finally 40 μg/mL (20 mm in diameter) making an inhibition zone of 36 ± 1.2 mm and 37 ± 1 mm for *S. aureus* and *E. coli*, respectively. According to the standard 195920-ASTM E2149-01 (Kavoosi et al., 2013) all disks showed antibacterial effects, since the zone of inhibition exceeds 1 mm.

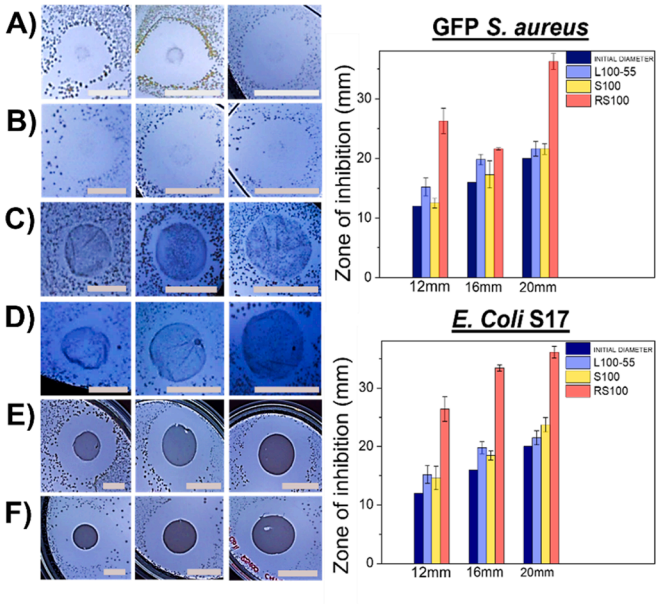

Fig. 5. Representative images of antimicrobial disk diffusion test for L100-55/CHXD (A), S100/CHXD (C) and RS100/CHXD (E) against *S. aureus* and L100-55/CHXD (B), S100/CHXD (D) and RS100/CHXD (F) against *E. coli* after 24 h. Plots of the measurements of the disk and their antimicrobial effect. Scale bar: 10 mm.

3.6. Cytocompatibility assays

The cytocompatibility of the synthesized dressings was assayed in J774 macrophages at the cell metabolism level by the Blue® Cell Viability Assay. Cells were exposed to 4 mg/mL of the different drug-loaded dressings described above. The results obtained were compared

with cells not treated (control for the evaluation of the free drugs) or with cells treated with the appropriate non-loaded dressing (control for the evaluation of drug-loaded dressings).

As depicted in Fig. 6, free drugs attained low viability percentages at their loaded concentrations in the dressings, showing percentages lower than 60% being chlorhexidine the drug that exerted the most detrimental effects in cells. The treatment of J774 cells with the loaded dressings for 24 h displayed viability percentages higher than 80% in the case of RIF being RIF-loaded RS100 dressings the most cytocompatible ones showing percentages as the ones retrieved for the control sample (~100%). CHXD-loaded dressings showed viabilities higher than 70% except for CHXD-loaded RS100 whose percentage was slightly lower (~65%). THY loaded dressings displayed the lowest viability percentages (<70%) classifying the material loaded at that THY concentration as cytotoxic (according to the value established by the ISO 10993–5) while RIF and CHXD dressings fulfil the requirements of this ISO standard (ISO).

Our results revealed a significant higher cellular viability when using drug-loaded membranes vs cell treatment with the free compounds highlighting the efficiency of drug encapsulation to fulfil a sustained release decreasing cytotoxicity.

RIF is a well-known broad spectrum antibiotic which is administered to treat a wide range of pathogenic bacterial infections. Our results displayed high cytocompatibility of RIF-loaded membranes pointing to their suitability for biomedical purposes as previous studies have also demonstrated. RIF-loaded PCL tridimensional scaffolds exerted cellular viabilities on human osteoblasts close to the ones obtained for the untreated control sample at different RIF and polymer concentrations after 24 h of incubation even when the scaffold exerted a drug release higher than 1 mg/mL, concentration much higher than ours (≤42 μg/mL) (Lee et al., 2020). In this sense, chitosan and extracellular matrix derived proteins at different ratios were used to fabricate scaffolds loaded with RIF (0.5 mg per scaffold) which also showed low cytotoxicity on HMEC-1 cells though the drug release profiles from the scaffolds are not shown (Goller and Turner, 2020). Previous studies in our group have also evidenced these results when human osteoblasts were seeded directly onto PCL scaffolds loaded with PLGA microparticles containing RIF whose drug release was significantly higher than the one provided by the current dressings (96–148 μg/mL vs ≤ 42 μg/mL) (Aragón et al., 2019). The antiseptics THY and CHXD exerted more harmful effects as expected due to their non-selective antiseptic character. J774 macrophages treated with PCL scaffolds loaded with THY during 24 h showed also low viability percentages (<50%) but higher than those percentages obtained from samples treated with the equivalent dose of the free compound (Aragón et al., 2019). THY release from these scaffolds (60–90 μg/mL) was in the range of ours (27–194 μg/mL). Scaffolds embedded in CHXD solution (polyethylene terephthalate modified by chitosan crosslinked with genipin) were tested in L132 cell cultures exerting similar results to ours but after 3 days of incubation and with a higher drug release during the first 24 (Aubert-Viard et al., 2019). In addition, CHXD coatings on silica nanoparticles incorporated into a commercial formulation of a poly(methyl methacrylate) (PMMA) bone cement (Cemex®) resulted in high viability percentages (>70%) when Saos-2 cells were cultured with the released medium of these complexes though a low drug release was observed (Al Thaher Y et al., 2021). Skin regeneration after wound infection and subsequent treatment with an antiseptic involves the removal of pathogenic bacteria but also some skin cells. However, new cells are recruited to the damaged area owing to the immune response in order to regenerate the tissues and therefore, repair the skin. Therefore, after the elimination of pathogenic bacteria macrophages, fibroblasts and endothelial cells are recruited to initiate the regenerative process: cell proliferation, migration and regeneration.

4. Conclusions

Smart wound dressings having pH-responsiveness have been developed in order to tune drug release kinetics depending on the needs of the wound in the different stages of wound healing. In the prophylaxis against infection development on intact skin having a pH of 5.5, RIF loaded-L100-55 composing dressings would release the loaded antibiotic immediately eliminating any potential pathogenic bacteria present from colonizing the wound. In the management of infected chronic wounds (i.e., having alkaline pH) CHXD-loaded L100-55 composing dressings would be recommended because they would release the antiseptic over time reaching a maximum under alkaline conditions. Finally, in the management of acute wounds (i.e., having neutral pH) RIF-loaded S100 composing fibers would be recommended showing a sustained release reaching a maximum under neutral pH. An efficient antimicrobial action against gram positive and gram negative bacteria was observed while the cytotoxicity against eukaryotic cells is reduced when the antimicrobial was incorporated into the dressings compared to the effect of the free compounds.

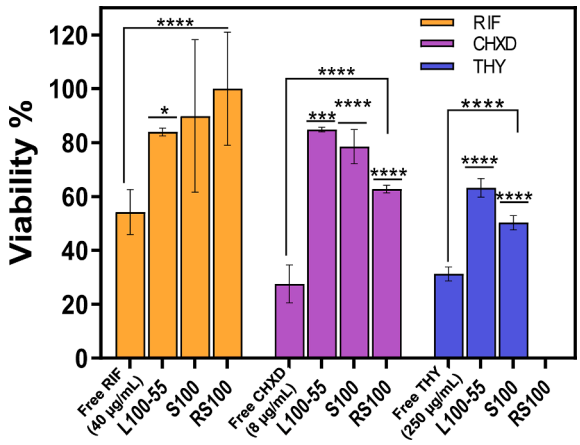

Fig. 6. Cell viability in the J774 cell line of RIF, CHXD and THY loaded fibers of L100-55, S100 and RS100 compared to the equivalent dose of the free antimicrobial compound. 100% viability of each free drug was assigned to the untreated control cells and for each loaded fiber, the non-loaded fibers were also used as control samples for the drug-loaded membranes. Data are presented as mean ± SD (n = 3). Significant statistical differences between the free drug and the loaded dressings are depicted in brackets while the differences between each membrane and the loaded one are depicted above each column (*p < 0.05; ***p < 0.01; ****p < 0.0001).

CRediT authorship contribution statement

Laura Miranda-Calderon: Investigation. **Cristina Yus:** Investigation, Methodology. **Guillermo Landa:** Investigation. **Gracia Mendoza:** Conceptualization, Methodology, Writing – review & editing. **Manuel Arruebo:** Conceptualization, Writing – review & editing, Funding acquisition. **Silvia Irusta:** Conceptualization, Writing – review & editing, Funding acquisition.

Declaration of Competing Interest

The authors declare that they have no known competing financial interests or personal relationships that could have appeared to influence the work reported in this paper: [Guillermo Landa reports financial support provided by Spain Ministry of Science and Innovation. Silvia Irusta reports financial support provided by Spain Ministry of Science and Innovation. Gracia Mendoza reports financial support provided by Carlos III Health Institute. Laura Miranda-Calderon reports financial support provided by National Council on Science and Technology. Manuel Arruebo reports financial support provided by Spain Ministry of Science and Innovation.].

Acknowledgements

This research was funded by the Spanish Ministry of Science and Innovation (grant number PID2020-113987RB-I00). G.L. acknowledges the support from the FPI fellowship PRE2018-085769 granted by the Spanish Ministry of Science, Innovation and Universities, while L.G.M-C. acknowledges the financial support from the Mexican Council of Science and Technology (CONACyT) through doctoral grant #710618. G.M. gratefully acknowledges the support from the Miguel Servet Program (MS19/00092; Instituto de Salud Carlos III). CIBER-BBN is an initiative funded by the VI National R&D&i Plan 2008 -2011, Iniciativa Ingenio 2010, Consolider Program, CIBER Actions and financed by the Instituto de Salud Carlos III (Spain) with assistance from the European Regional Development Fund.

References

Al-Ani, E., Martin, C., Britland, S.T., Doudin, K., Hill, D.J., 2019. The effect of the source and the concentration of polymers on the release of chlorhexidine from mucoadhesive buccal tablets. Saudi Pharm. J. 27 (6), 756–766.

Al Thaher, Y., Alotaibi, H.F., Yang, L., Prokopovich, P., 2021. PMMA bone cement containing long releasing silica-based chlorhexidine nanocarriers. PLoS ONE 16, e0257947.

Aragón, J., Feoli, S., Irusta, S., Mendoza, G., 2019. Composite scaffold obtained by electro-hydrodynamic technique for infection prevention and treatment in bone repair. Int. J. Pharm. 557, 162–169.

Attinger, C., Wolcott, R., 2012. Clinically addressing biofilm in chronic wounds. Adv. Wound Care (New Rochelle) 1 (3), 127–132.

Aubert-Viard, F., Mogrovejo-Valdivia, A., Tabary, N., Maton, M., Chai, F., Neut, C., Martel, B., Blanchemain, N., 2019. Evaluation of antibacterial textile covered by layer-by-layer coating and loaded with chlorhexidine for wound dressing application. Mater. Sci. Eng. C, Mater. Biol. Applications 100, 554–563.

Bigliardi, P.L., Alsagoff, S.A.L., El-Kafrawi, H.Y., Pyon, J.-K., Wa, C.T.C., Villa, M.A., 2017. Povidone iodine in wound healing: a review of current concepts and practices. Int. J. Surgery 44, 260–268.

Bowler, P.G., Duerden, B.I., Armstrong, D.G., 2001. Wound microbiology and associated approaches to wound management. Clin. Microbiol. Rev. 14 (2), 244–269.

Chen, L., Bromberg, L., Hatton, T.A., Rutledge, G.C., 2008. Electrospun cellulose acetate fibers containing chlorhexidine as a bactericide. Polymer 49 (5), 1266–1275.

Drapeau, C.M.J., Grilli, E., Petrosillo, N., 2010. Rifampicin combined regimens for gram-negative infections: data from the literature. Int. J. Antimicrob. Agents 35 (1), 39–44.

ISO 10993, 2009. Biological evaluation of medical devices — Part 5: Tests for in vitro cytotoxicity.

ECHA, 2011. https://echa.europa.eu/documents/10162/b21b9828-ff70-ccd6-ae3d-96c4420b99c7.

Edmonds, M., Manu, C., Vas, P., 2021. The current burden of diabetic foot disease. J. Clin. Orthopaedics Trauma 17, 88–93.

Filgueiras, A.L., Lima, F.R.A., de Carvalho, D.F., Meirelles, M.A., Paschoal, D., dos Santos, H.F., Sanchez-Cortes, S., Sant'Ana, A.C., 2016. The adsorption of rifampicin on gold or silver surfaces mediated by 2-mercaptoethanol investigated by surface-enhanced Raman scattering spectroscopy. Vib. Spectrosc. 86, 75–80.

Gámez-Herrera, E., García-Salinas, S., Salido, S., Sancho-Albero, M., Andreu, V., Pérez, M., Luján, L., Irusta, S., Arruebo, M., Mendoza, G., 2020. Drug-eluting wound dressings having sustained release of antimicrobial compounds. Eur. J. Pharm. Biopharm. 152, 327–339.

Gámez, E., Elizondo-Castillo, H., Tascon, J., García-Salinas, S., Navascues, N., Mendoza, G., Arruebo, M., Irusta, S., 2020. Antibacterial Effect of Thymol Loaded SBA-15 Nanorods Incorporated in PCL Electrospun Fibers. Nanomaterials 10 (4), 616.

Gámez, E., Mendoza, G., Salido, S., Arruebo, M., Irusta, S., 2019. Antimicrobial electrospun polycaprolactone-based wound dressings: an in vitro study about the importance of the direct contact to elicit bactericidal activity. Adv. Wound Care (New Rochelle) 8 (9), 438–451.

Garcia-Salinas, S., Gámez, E., Landa, G., Arruebo, M., Irusta, S., Mendoza, G., 2020. Antimicrobial wound dressings against fluorescent and methicillin-sensitive intracellular pathogenic bacteria. ACS Appl. Mater. Interfaces 12 (46), 51302–51313.

Gilchrist, S.E., Lange, D., Letchford, K., Bach, H., Fazli, L., Burt, H.M., 2013. Fusidic acid and rifampicin co-loaded PLGA nanofibers for the prevention of orthopedic implant associated infections. J. Control. Release 170 (1), 64–73.

Giménez-Martín, E., López-Andrade, M., Ontiveros-Ortega, A., Espinosa-Jiménez, M., 2009. Adsorption of chlorhexidine onto cellulosic fibers. Cellulose 16 (3), 467–479.

Goller, S., Turner, N.J., 2020. The antimicrobial effectiveness and cytotoxicity of the antibiotic-loaded chitosan. ECM Scaffolds 10, 3446.

Haller, H.L., Sander, F., Popp, D., Rapp, M., Hartmann, B., Demircan, M., Nischwitz, S.P., Kamolz, L.P., 2021. Oxygen, pH, lactate, and metabolism—how old knowledge and new insights might be combined for new wound treatment. Medicina 57, 1190.

Holešová, S., Samlíková, M., Ritz, M., Pazdziora, E., 2015. Antibacterial polyethylene/clay nanocomposites using chlorhexidine as organic modifier. Mater. Today: Proc. 2, 246–252.

Ibrahim, H.M., Klingner, A., 2020. A review on electrospun polymeric nanofibers: production parameters and potential applications. Polym. Test. 90, 106647.

Jones, E.M., Cochrane, C.A., Percival, S.L., 2015. The effect of pH on the extracellular matrix and biofilms. Adv. Wound Care (New Rochelle) 4, 431–439.

Juven, B.J., Kanner, J., Schved, F., Weisslowicz, H., 1994. FACTORS that interact with the antibacterial action of thyme essential oil and its active constituents. J. Appl. Bacteriol. 76, 626–631.

Kadam, S., Shai, S., Shahane, A., Kaushik, K.S., 2019. Recent advances in non-conventional antimicrobial approaches for chronic wound biofilms: have we found the 'Chink in the Armor'? Biomedicines 7, 35.

Kalan, L., Grice, E.A., 2018. Fungi in the Wound Microbiome. Adv. Wound Care (New Rochelle) 7, 247–255.

Kavoosi, G., Dadfar, S.M., Purfard, A.M., 2013. Mechanical, physical, antioxidant, and antimicrobial properties of gelatin films incorporated with thymol for potential use as nano wound dressing. J. Food Sci. 78, E244–E250.

Kramer, A., Dissemond, J., Kim, S., Willy, C., Mayer, D., Papke, R., Tuchmann, F., Assadian, O., 2018. Consensus on Wound Antisepsis: Update 2018. Skin Pharmacol. Physiol. 31, 28–58.

Lee, J.-H., Baik, J.-M., Yu, Y.-S., Kim, J.H., Ahn, C.B., Son, K.H., Kim, J.-H., Choi, E.S., Lee, J.W., 2020. Development of a heat labile antibiotic eluting 3D printed scaffold for the treatment of osteomyelitis. Sci. Rep. 10, 7554.

Lessa, F.C., Nogueira, I., Vargas Fda, S., Spolidorio, D.M., Hebling, J., García-Godoy, F., Costa, C.A., 2010. Direct and transdentinal antibacterial activity of chlorhexidine. Am. J. Dent. 23, 255–259.

Liu, X., Ma, X., Kun, E., Guo, X., Yu, Z., Zhang, F., 2018. Influence of lidocaine forms (salt vs. freebase) on properties of drug–eudragit® L100–55 extrudates prepared by reactive melt extrusion. Int. J. Pharm. 547, 291–302.

Luddin, N., Ahmed, H.M.A., 2013. The antibacterial activity of sodium hypochlorite and chlorhexidine against Enterococcus faecalis: a review on agar diffusion and direct contact methods. J. Conserv. Dent 16, 9–16.

Lukic, I., Vulic, J., Ivanovic, J., 2020. Antioxidant activity of PLA/PCL films loaded with thymol and/or carvacrol using $scCO_2$ for active food packaging. Food Packaging Shelf Life 26, 100578.

Martín-Illana, A., Cazorla-Luna, R., Notario-Pérez, F., Bedoya, L.M., Rubio, J., Tamayo, A., Ruiz-Caro, R., Veiga, M.D., 2021. Smart vaginal bilayer films of Tenofovir based on Eudragit® L100/natural polymer for the prevention of the sexual transmission of HIV. Int. J. Pharm. 602, 120665.

McCarty, S.M., Percival, S.L., 2013. Proteases and Delayed Wound Healing. Adv. Wound Care (New Rochelle) 2, 438–447.

Meechaisue, C., Dubin, R., Supaphol, P., Hoven, V.P., Kohn, J., 2006. Electrospun mat of tyrosine-derived polycarbonate fibers for potential use as tissue scaffolding material. J. Biomater. Sci. Polym. Ed. 17, 1039–1056.

Obeidat, W.M., Price, J.C., 2003. Viscosity of polymer solution phase and other factors controlling the dissolution of theophylline microspheres prepared by the emulsion solvent evaporation method. J. Microencapsul. 20, 57–65.

Koester, D., 2018. Standard Test Method for Determining the Activity of Incorporated Antimicrobial Agent (s) in Polymeric or Hydrophobic Materials.

Olsson, M., Järbrink, K., Divakar, U., Bajpai, R., Upton, Z., Schmidtchen, A., Car, J., 2019. The humanistic and economic burden of chronic wounds: a systematic review. Wound Repair Regen 27, 114–125.

Patra, C., Priya, R., Swain, S., Jena, G.K., Panigrahi, K.C., Ghose, D.J.F., 2017. Pharmaceutical significance of Eudragit: a review. Future J. Pharm. Sci. 3, 33–45.

Pignatello, R., Amico, D., Chiechio, S., Spadaro, C., Puglisi, G., Giunchedi, P., 2001. Preparation and analgesic activity of Eudragit RS100 microparticles containing diflunisal. Drug Delivery 8, 35–45.

Reda, R.I., Wen, M.M., El-Kamel, A.H., 2017. Ketoprofen-loaded Eudragit electrospun nanofibers for the treatment of oral mucositis. Int. J. Nanomed. 12, 2335–2351.

Roberts, C.D., Leaper, D.J., Assadian, O., 2017. The role of topical antiseptic agents within antimicrobial stewardship strategies for prevention and treatment of surgical site and chronic open wound infection. Adv. Wound Care (New Rochelle) 6, 63–71.

Saraiva, A.G.Q., Saraiva, G.D., Albuquerque, R.L., Nogueira, C.E.S., Teixeira, A.M.R., Lima, L.B., Cruz, B.G., de Sousa, F.F., 2020. Chemical analysis and vibrational spectroscopy study of essential oils from Lippia sidoides and of its major constituent. Vib. Spectrosc. 110, 103111.

Schloss, P.D., Handelsman, J., 2004. Status of the microbial census. Microbiol. Mol. Biol. Rev.: MMBR 68, 686–691.

Shiferaw, W.S., Akalu, T.Y., Mulugeta, H., Aynalem, Y.A., 2020. The global burden of pressure ulcers among patients with spinal cord injury: a systematic review and meta-analysis. BMC Musculoskeletal Disorders 21, 334.

Suci, P.A., Geesey, G.G., Tyler, B.J., 2001. Integration of Raman microscopy, differential interference contrast microscopy, and attenuated total reflection Fourier transform infrared spectroscopy to investigate chlorhexidine spatial and temporal distribution in Candida albicans biofilms. J. Microbiol. Methods 46, 193–208.

Taeger, C.D., Wallner, S., Martini, T., Schiltz, D., Kehrer, A., Prantl, L., Biermann, N., 2021. Analysis of rinsing fluid during negative pressure wound therapy with instillation: a potential monitoring tool in acute and chronic wound treatment. A Pilot Study. 10, 732.

Velnar, T., Bailey, T., Smrkolj, V., 2009. The wound healing process: an overview of the cellular and molecular mechanisms. J. Int. Med. Res. 37, 1528–1542.

Wiegand, C., Abel, M., Ruth, P., Elsner, P., Hipler, U.C., 2015. pH influence on antibacterial efficacy of common antiseptic substances. Skin Pharmacol. Physiol. 28, 147–158.
Xia, W., Razi, M.R.M., Ashley, P., Neel, E.A.A., Hofmann, M.P., Young, A.M., 2014. Quantifying effects of interactions between polyacrylic acid and chlorhexidine in dicalcium phosphate – forming cements. J. Mater. Chem. B 2, 1673–1680.
Zeng, J., Zhao, Y., Li, K., Long, D., Li, W., Liang, L., 2021. A coordinated ruthenium-rifampicin complex reprogramming the colon carcinoma micro-environment mediated by modulation of p53/AkT/mTOR/VEGF pathway. Toxicol. Appl. Pharmacol. 426, 115618.